Letter

Intermodulation of optical frequency combs in a multimode optomechanical system

Ryan C. Ng,[1,*] Paul Nizet,[1,*] Daniel Navarro-Urrios,[2] Guillermo Arregui,[3] Marcus Albrechtsen,[3] Pedro D. García,[1] Søren Stobbe,[3,4] Clivia M. Sotomayor-Torres,[1,5] and Guilhem Madiot[1,†]

[1]*Catalan Institute of Nanoscience and Nanotechnology (ICN2), Campus UAB, Bellaterra, 08193 Barcelona, Spain*
[2]*MIND-IN2UB, Departament d'Electrónica, Facultat de Física, Universitat de Barcelona, Martí i Franquès 1, Barcelona 08028, Spain*
[3]*DTU Electro, Department of Electrical and Photonics Engineering, Technical University of Denmark, ørsteds Plads 343, DK-2800 Kgs. Lyngby, Denmark*
[4]*NanoPhoton—Center for Nanophotonics, Technical University of Denmark, Ørsteds Plads 345A, DK-2800 Kgs. Lyngby, Denmark*
[5]*ICREA—Institució Catalana de Recerca i Estudis Avançats, 08010 Barcelona, Spain*

(Received 3 March 2023; revised 16 May 2023; accepted 2 August 2023; published 25 August 2023)

Phonons offer the possibility to connect the microwave and optical domains while being efficiently transduced with electronic and optical signals. Here, we present a multimodal optomechanical platform, consisting of a mechanical-optical-mechanical resonator configuration. The mechanical modes, with frequencies at 265 MHz and 6.8 GHz, can be simultaneously excited into a phonon lasing regime as supported by a stability analysis of the system. Both the megahertz and gigahertz modes enter a self-sustained oscillation regime, leading to the intermodulation of two frequency combs in the optical field. We characterize this platform experimentally, demonstrating previously unexplored dynamical regimes. These results suggest the possibility to control multiple mechanical degrees of freedom via a single optical mode, with implications in gigahertz phononic devices, signal processing, and optical comb sensing applications.

DOI: 10.1103/PhysRevResearch.5.L032028

I. INTRODUCTION

Phonons exist over an extremely broad frequency range from the Hertz to the terahertz regime. The control of phonons is difficult, especially at higher frequencies, despite the implications that such control would enable. For example, in the gigahertz regime, this could enable phonon signal processing, nanoacoustic devices, or hybrid quantum systems such as superconducting qubits [1–3]. Recent advances in the realization of high-frequency nanoacoustic devices have further motivated the extension of concepts from electronics and photonics to the realm of phononics [4–9]. In this context, cavity optomechanics provides a route toward the manipulation and control of phononic states via radiation-pressure forces [10–12]. Increasingly complex functionalities have been demonstrated in multimode optomechanical systems, where multiple optical and mechanical degrees of freedom interact [13–17]. Previously, several singular nonlinear phenomena have arisen from *self-pulsing* (SP), involving collective dynamics between free carriers and temperature in an optical cavity [18]. Such dynamics can produce rich dynamics, such as chaos [19], injection-locking [20], or frequency combs [21], but remain limited in frequency due to the relatively low thermalization rates encountered in these systems, which are typically on the order of a few tens of megahertz.

Intermodulation between mechanical spectra generally occurs in optomechanical experiments [22] over a limited range of the parameter space and does not involve highly nonlinear oscillations that produce optomechanical frequency combs. Here, we report an unexplored optomechanical dynamical regime that stems from the simultaneous self-sustained optomechanical oscillation of two mechanical modes that are far apart in frequency, leading to the intermodulation of two coherent processes which spectrally corresponds to the imbrication of two optical frequency combs. This mechanical-optical-mechanical (MOM) configuration is experimentally realized in a two-dimensional (2D) membrane phononic crystal (PnC) cavity waveguide sustaining both a 7 GHz phononic waveguide mode and a 265 MHz in-plane mechanical breathing mode of the full structure. Although thermal nonlinearities also exist in this optomechanical waveguide structure, the dynamics of the system is dictated purely by optomechanical interactions, which we confirm theoretically using a multimode optomechanical model. Consequently, the dynamics are set by mechanical properties of the structure that can be engineered over much shorter timescales than that of thermal effects. The multimodal interaction observed in this system leads to the formation and intermodulation of optical frequency combs in the gigahertz domain, with implications for atomic force and mass sensing [21,23–25].

II. MODEL

The archetypical representation of an optomechanical cavity uses an optical Fabry-Pérot cavity formed by two parallel

[*]These authors contributed equally to this work.
[†]Corresponding author

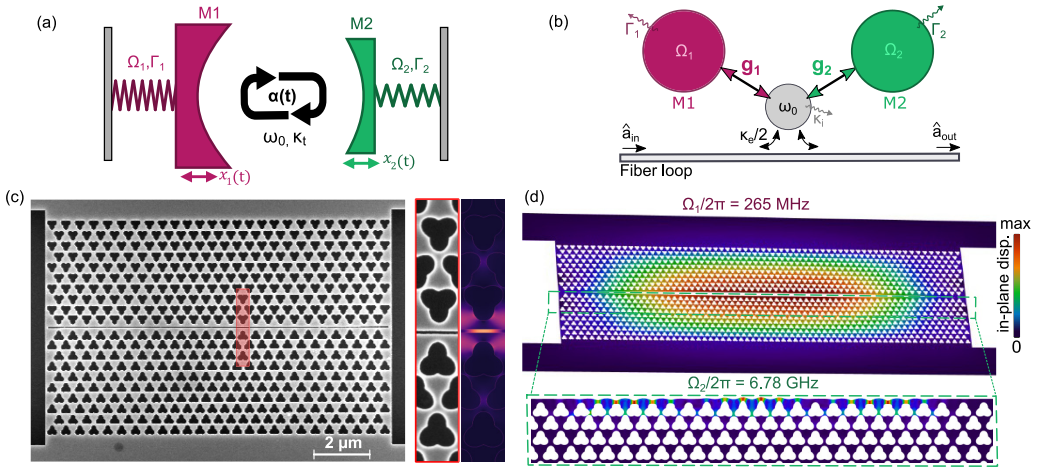

FIG. 1. Mechanical-optical-mechanical (MOM) modal configuration. (a) Generalized and (b) input-output schematic of a MOM multimodal configuration, where two mechanical modes (*M1* in red and *M2* in green) couple to a waveguide-coupled single optical mode via their respective optomechanical coupling rates. The optical mode is not explicitly represented in (a) and is highlighted in gray in (b). (c) A scanning electron microscope image of the optomechanical experimental realization using suspended silicon nanomembranes. A zoom-in shows the slotted optical waveguide and a finite-difference time-domain (FDTD) simulation of the electromagnetic energy confined within it. (d) Displacement field distribution of the low-frequency in-plane mechanical mode *M1* (top) and of the third-harmonic standing-wave acoustic mode traveling at the interface with the slot (bottom).

mirrors, one of which has a mechanical degree of freedom, such as via attachment to a spring. Figure 1(a) presents an adaptation of this representation to the MOM configuration, in this case using two moving mirrors. Each mirror (or mechanical mode) *Mi* has its own natural mechanical frequency Ω_i and damping rate Γ_i and couples to the optical field with a single-photon optomechanical coupling g_i. Their displacement is given by $x_i(t)$. An alternative input-output representation to more clearly observe intermode coupling is shown in Fig. 1(b), where an optical waveguide (represented here by a fiber loop that is used in the experiment later on in this letter) is side-coupled to an optical mode which interacts with *M1* and *M2*. The optical mode has a total decay rate $\kappa_t = \kappa_i + \kappa_e$, where κ_e is the decay rate associated with the input channel, and κ_i is the decay rate due to intrinsic losses. The linearized classical equations of motion for the cavity amplitude α and for the mechanical displacements x_1 and x_2 can be expressed as

$$\begin{aligned}\dot{\alpha} &= \left[j(\Delta + g_1 x_1 + g_2 x_2) - \frac{\kappa_t}{2}\right]\alpha + \sqrt{\frac{\kappa_e}{2}}s_{\text{in}},\\ \ddot{x_1} &= -\Gamma_1 \dot{x_1} - \Omega_1^2 x_1 + 2\Omega_1 g_1 |\alpha|^2,\\ \ddot{x_2} &= -\Gamma_2 \dot{x_2} - \Omega_2^2 x_2 + 2\Omega_2 g_2 |\alpha|^2,\end{aligned} \tag{1}$$

where $\Delta = \omega_\ell - \omega_0$ is the detuning between the laser frequency $\omega_\ell = 2\pi c/\lambda$ and the cavity resonance frequency ω_0, and s_{in} is the input laser field amplitude, such that $P_{\text{in}} = \hbar\omega_\ell |s_{\text{in}}|^2$ is the laser input power. Note that the displacements are normalized by the zero-point fluctuation of each of the mechanical modes such that the mechanical masses can be eliminated. In a standard optomechanical cavity, the mechanical susceptibility, which describes the mechanical spectral response to an external perturbation, is altered by the laser field such that a *direct* modification of both the mechanical frequency and damping occurs [26]. When considering a second mechanical mode, a correction term to each mechanical susceptibility can be derived (see Supplemental Material [27]). This *indirect* modification leads to gain competition between the two mechanical modes by acting against the direct optomechanical effect and therefore increases the threshold powers at which each mode can enter a self-sustained oscillation regime [28,29]. When $\Omega_1 \sim \Omega_2$, simultaneous phonon lasing of both modes generally cannot occur, although it can be achieved using external modulation of the laser [30]. This case of nearly degenerate mechanical modes implies that they couple to one another through light, leading to hybridization of the modes as observed in a SiN membrane placed inside an optical fiber cavity [31]. The study of exceptional points [32], which analyzes how gain and loss within a system can be balanced, has also been made possible using such a MOM configuration [14], although the phonon lasing regime was not observed. When $\Omega_1 \ll \Omega_2$, the coupling between *M1* and *M2* becomes nonresonant which allows for simultaneous lasing of the two mechanical modes at a relatively small input power and leads to the formation and intermodulation of combs that will subsequently be described.

III. EXPERIMENTAL REALIZATION

While the underlying physics of such a multimode system are general, one example design in which the MOM configuration can be experimentally reproduced is in a 220-nm-thick suspended silicon membrane fabricated in silicon-on-insulator with etched shamrock-shaped holes that form a 2D PnC displaying wide acoustic band gap ~6 GHz [33]. Two PnCs with mirror symmetry are brought together and separated by a thin 40-nm-wide air-slot within which light can be confined. Figure 1(c) shows a scanning electron microscope (SEM) image of the PnC/air-slot/PnC platform with a zoom-in of the red-shaded rectangle emphasizing the air-slot provided on the right. A finite-element-method

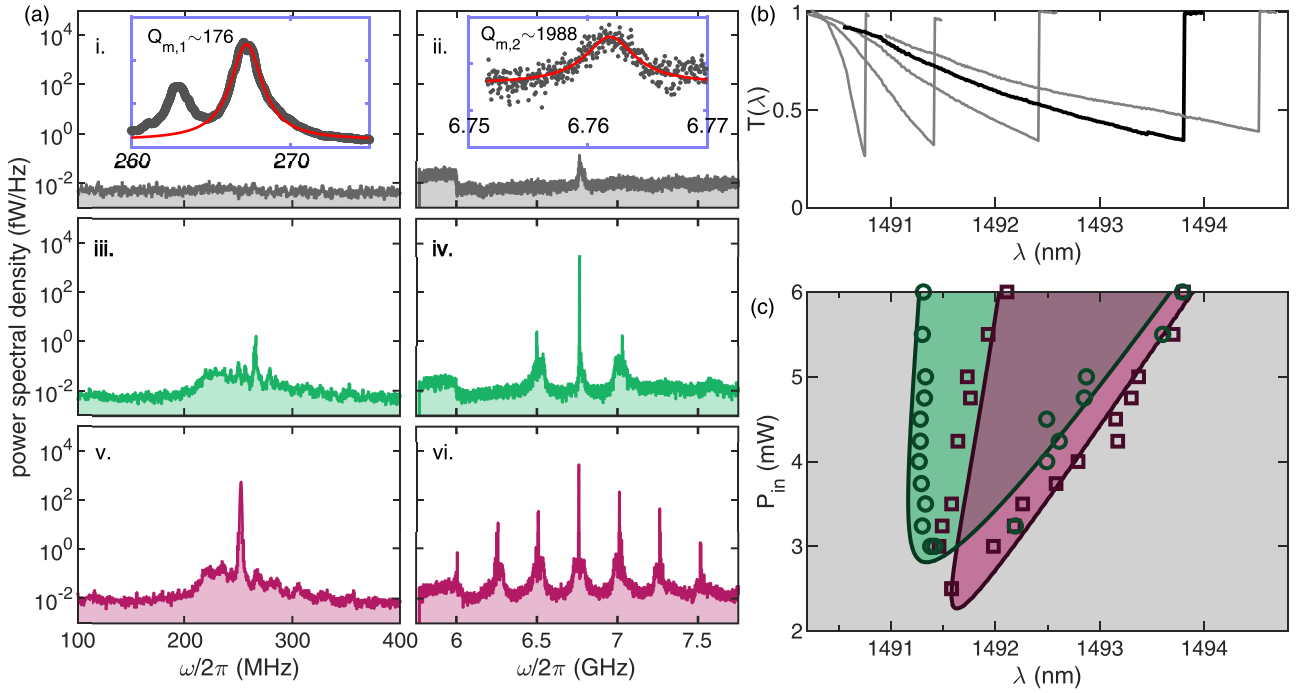

FIG. 2. Observed physical regimes. (a) Mechanical RF spectra for the (i), (iii), and (v) megahertz range and (ii), (iv), and (vi) gigahertz range. Three characteristic dynamical regimes are observed: thermal (gray), *M1* lasing (red), and *M2* lasing (green), and comb intermodulation (overlap of red and green regions), which results from simultaneous *M1* and *M2* lasing. Insets in (i) and (ii) show averaged spectra (gray) each fitted with a Lorentzian (red). (b) Transmission response measured by driving a localized optical mode with a tunable laser from the blue-detuned side, using $P_{\text{in}} = 4.5$ mW. (c) Theoretical map highlighting the lasing thresholds for *M1* and *M2* as a function of the laser power and wavelength. The thresholds are shown with solid lines. The gray, green, and red areas correspond to both modes in the thermal regime, *M2* lasing ($\Gamma_{\text{eff},2} < 0$), and *M1* lasing ($\Gamma_{\text{eff},1} < 0$), respectively. The experimentally determined thresholds of *M2* (green circles) and *M1* (red squares) are overlaid.

simulation of the optical field energy density confined in the air-slot is also shown. Inherent fabrication imperfections such as etched sidewall roughness [34] lead to disorder-induced spatially localized optical modes. From hereon, we are implicitly referring to these disorder-induced optical modes when mentioning optical modes in our structure. The localized modes provide efficient optomechanical transduction (i.e., the ability to couple light to mechanical motion) due to their high quality factors and small effective mode volumes, without the need to carefully design a confinement potential [35]. The exact geometric parameters of the crystal can be found in the Supplemental Material [27], and further details regarding fabrication and design of the optomechanical structure are found in Madiot *et al.* [36]. We define two mechanical modes observed in this structure as *M1* and *M2*, referring to the mechanical modes in the megahertz and gigahertz regimes, respectively. In the structure explored here, *M1* corresponds to the fundamental mechanical breathing mode in the megahertz regime, or vibrations along the entire length of the plates, which strongly couples to the optical field in the slot, making it ideal for cavity optomechanical systems [35,37–39]. Here, *M2* corresponds to a stationary wave resulting from the confinement of a mechanical guided mode in the acoustic Fabry-Pérot cavity formed on one side of the slot and between the two acoustic mirrors at the edges [33,36]. The in-plane components of the displacement fields associated with *M1* and *M2* are shown in Fig. 1(d). Both modes couple to the same optical mode, although they are unlikely to couple directly to one another, as the overlap of the displacement fields is weak due to the large difference in length scale and frequency. Since the two plates are identical and independent, each would sustain a gigahertz mechanical mode, although they are not readily differentiated here. By using a tapered-fiber loop brought into contact with the optical waveguide, these telecom-wavelength optical modes can be driven to transduce both of these megahertz and gigahertz mechanical modes.

IV. RESULTS AND DISCUSSION

A localized optical mode is resonantly driven by injecting light from a tunable laser with input power $P_{\text{in}} = 5.0$ mW in the fiber loop. The position of the loop for coupling to the mode and the polarization of the input light are optimized by maximizing the thermo-optic broadening of the mode, observed when scanning the lasing wavelength upward. The output field is analyzed with a fast photoreceiver connected to an electrical spectrum analyzer. As the optical mode is driven at increasing coupling fractions by varying Δ, different physical regimes are observed, summarized in their respective power spectral densities in Fig. 2(a) for the megahertz (left panels) and the gigahertz (right panels) regimes. By approaching the optical mode with a blue-detuned laser, the first regime is a thermal regime in which both modes are thermally excited (gray), although only *M2* is transduced at first. As the coupling mode fraction in the driven optical mode increases, a second regime appears in which a single gigahertz mechanical lasing

peak is observed for *M2* with sidebands formed by a thermally excited *M1* in the megahertz regime (green region). At this point, several other mechanical modes in the megahertz regime are observed. Due to the number of modes, accurate determination of the spectral linewidth of *M1* is impeded, especially at coupling fractions which are sufficient to guarantee the absence of any dynamical backaction. This is the main limiting factor for the determination of the optomechanical coupling g_1. For an even greater coupling fraction, *M1* also enters a self-sustained oscillation regime (red region). The exponentially growing oscillations that result from an optomechanical instability saturate due to nonlinear effects. This process eventually leads to the emergence of various harmonics when driving the oscillator significantly above its lasing threshold. The resulting spectral feature is an optical frequency comb [40,41]. When both modes lase (region in which the red and green regions overlap), the lasing of *M1* in the megahertz regime modulates the principal lasing peak of *M2* in the gigahertz regime, giving rise to a frequency comb centered at $\Omega_2/2\pi = 6.764\,\text{GHz}$ with spacing equal to $\Omega_1/2\pi = 265\,\text{MHz}$. The transmission optical spectrum associated with these measurements is shown in Fig. 2(b) (black line), accompanied by other scans at different input powers (gray lines). We observe additional broadening of the thermo-optically bistable resonance as P_{in} increases.

By scanning the laser wavelength λ over the resonance, we collect the lasing thresholds, or wavelengths at which the amplitude of each mode begins an exponential increase or decrease, for both mechanical modes (see Supplemental Material [27]). We determine the mechanical lasing thresholds of *M1* and *M2* at different powers and report them in Fig. 2(c) with red squares and green circles, respectively. The optomechanical interaction alters the mechanical susceptibilities as computed via Eq. (1) such that the effective mechanical damping rates $\Gamma_{\text{eff},i}$ can be extracted to determine the phonon lasing condition of each mode. To allow for direct comparison with experiment, the theoretical reduced laser detuning Δ incorporates a resonant-wavelength λ_0 that is corrected for any thermo-optic shifts of the resonant cavity frequency using $\lambda_0' = \lambda_0 + \eta|\alpha|^2$, where $\eta/\hbar\omega_\ell \approx 0.35$ nm/fJ is a static nonlinearity estimated from the experimental data (see Supplemental Material [27]). The cavity photon number $|\alpha|^2$ as a function of λ and P_{in} is numerically resolved by accounting for the static thermo-optic nonlinearity, and the solutions are entered into the effective susceptibility to determine the effective damping rates. The calibrated experimental parameters are $\lambda_0 = 1490.6$ nm, $\kappa_i/2\pi = 5.0\,\text{GHz}$, $\kappa_e/2\pi = 4.5\,\text{GHz}$, $\Gamma_1/2\pi = 1.5\,\text{MHz}$, and $\Gamma_2/2\pi = 3.4\,\text{MHz}$. Using a phase-modulation calibration method [42], we have determined the optomechanical coupling associated with *M2*, $g_2/2\pi = 260\,\text{kHz}$. From the mechanical frequencies and linewidths, the mechanical Q factors are $Q_{m,1} = \Omega_1/\Gamma_1 \approx 176$ and $Q_{m,2} = \Omega_2/\Gamma_2 \approx 1988$. Both linewidths are determined by driving another localized optical mode with $\lambda = 1489.9$ nm and $P_{\text{in}} = 0.2$ mW. The spectra are acquired with low-resolution bandwidth and higher averaging time and are each fitted with a Lorentzian, as shown in the insets of Figs. 2(a)(i) and 2(a)(ii). Similarly, we evaluate the optical Q factor $Q_{\text{opt}} = \omega_0/\kappa_t$, where $\omega_0 = 2\pi c/\lambda_0$ and $\kappa_t = \kappa_0 + \kappa_e$, which leads to $Q_{\text{opt}} \approx 21172$. Figure 2(c) indicates when $\Gamma_{\text{eff},1} < 0$ (green shaded region) and when $\Gamma_{\text{eff},2} < 0$ (red shaded region). Each of these regions is delineated by the lasing threshold of each mode, $\Gamma_{\text{eff},1} = 0$ and $\Gamma_{\text{eff},2} = 0$. The experimental results are numerically fitted with the theory using only g_1 as a fitting parameter, with g_2 being experimentally calibrated. We find the 95% confidence interval $g_1/2\pi = 480 \pm 10\,\text{kHz}$ which quantitatively captures the observed experimental values. This value is in good agreement with the optomechanical couplings found for the in-plane mechanical modes of similar slotted-waveguide optomechanical platforms [35]. The red region is mostly encompassed within the green one, representing a region in which simultaneous mode lasing occurs.

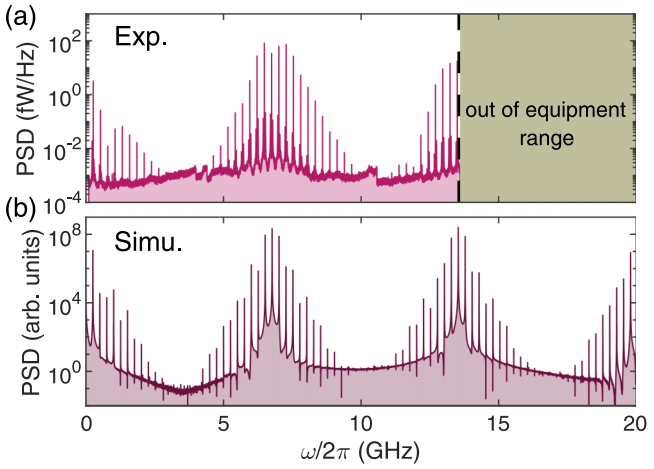

FIG. 3. RF spectrum over full spectral range. Power spectral density of the output optical field in the simultaneous lasing regime measured over the 0–13.5 GHz frequency range. Up to 10 pairs of sidebands on each side of Ω_2 are observed, while the second harmonic of this pattern (centered at $2\Omega_2$) is partially visible near the signal analyzer limit.

Figure 3(a) shows the power spectral density of the output optical field measured in the multimode lasing regime with a resolution bandwidth set to 50 kHz over the full span of the electrical spectrum analyzer from 0 to 13.5 GHz. Here, *M1* lases at 265 MHz, leading to the emergence of a first frequency comb with ~10 harmonics up to 2.650 GHz. Here, *M2* also lases, but the second harmonic already lies above the equipment limit. The harmonics of *M1* are imprinted in the frame rotating at Ω_2, such that ~10 pairs of sidebands are visible around Ω_2. This frequency pattern is duplicated in all the harmonics of *M2*, such that the beginning of its second occurrence (centered at $2\Omega_2$) can be spotted >12 GHz. This result is indicative of the observed multimodal intermodulation, as the gigahertz sidebands cannot occur in the absence of *M1* lasing (see Supplemental Material [27]). The experimental spectrum is plotted over the 0–20 GHz range for direct comparison with Fig. 3(b), which shows a numerical simulation. Both exhibit the same type of spectral structure with slight variations of the harmonic amplitude distribution.

Other regimes involving another megahertz mechanical mode as well as SP dynamics could also be observed within this structure for certain experimental input parameters but are ignored by our model. A SP regime with thermal oscillation at $\Omega_{\text{SP}}/2\pi = 13.5\,\text{MHz}$ is found in addition to simultaneous

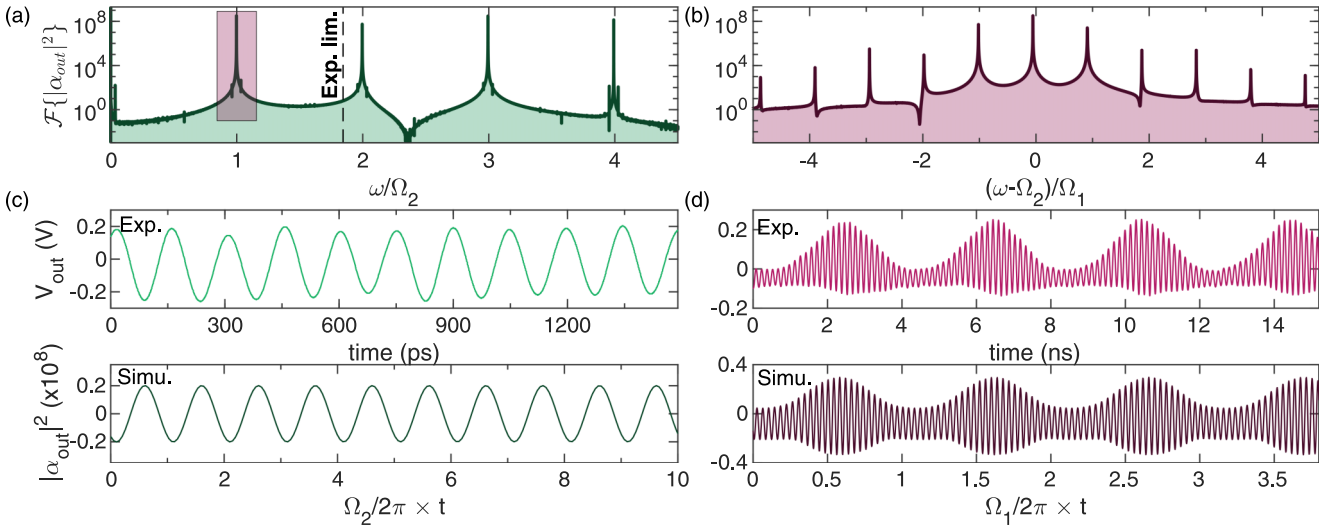

FIG. 4. Physical regimes in the time domain. Simulated Fourier spectrum of $|\alpha_{\text{out}}(t)|^2$ for (a) the *M2* lasing regime and (b) the comb intermodulation arising from simultaneous *M1* and *M2* lasing. The experimental measurement cutoff due of the measurement setup is indicated with a dashed line in (a). For comparison, the frequency range from (b) is highlighted in (a) by a red box. Experimental (top) and simulated (bottom) time traces are shown for the (c) *M2* lasing regime and (d) multimode lasing regime.

optomechanical lasing of *M1* and *M2*, leading to another level of intermodulation (see Supplemental Material).

The regimes where *M2* lases independently [Figs. 2(a)(iii)–2(a)(vi)] and where both modes lase simultaneously [Figs. 2(a)(v)–2(a)(vi)] are reproduced numerically using Eq. (1), and are shown in Figs. 4(a) and 4(b), respectively, using the output photon flux $|\alpha_{\text{out}}(t)|^2$, where $\alpha_{\text{out}} = s_{\text{in}} - \sqrt{\frac{\kappa_e}{2}}\alpha$ (see Supplemental Material [27]). The experimental oscilloscope cutoff frequency is at 8 GHz. The associated experimental (top) and simulated (bottom) time traces for each case are shown in Figs. 4(c) and 4(d). Our experimental apparatus is limited to 13.5 GHz [dashed line in Fig. 4(a)], which lies slightly below the second harmonic. Both of the associated time traces for this scenario [Fig. 4(c)] show slightly anharmonic oscillation at Ω_2. A low-pass filter with cutoff frequency at 8 GHz is applied to the simulation time traces (bottom) to reproduce the oscilloscope bandwidth. For the case where simultaneous lasing occurs [Fig. 4(b)], the frequency is centered at Ω_2 and normalized with Ω_1, indicating the presence of a comb centered at Ω_2 with spacing given by Ω_1. This spectrum shows three pairs of sidebands, which are also observed experimentally in Fig. 2(a)(vi). These correspond to the first four harmonics of *M1* that imprint in the frame rotating at Ω_2 via the indirect nonlinear coupling of the mechanical modes. These harmonics emerge when *M1* passes its lasing threshold, like the case of *M2*. The experimental time trace in Fig. 4(d) (top) shows amplitude modulation of the gigahertz tone by the megahertz tone, in the output optical field. The simulated trace (bottom) exhibits good qualitative agreement with experiment.

V. CONCLUSIONS

We presented a MOM multimodal optomechanical platform, connecting spectrally distant phonons and photons in the megahertz, gigahertz, and hundreds of terahertz regimes, and demonstrated optical control the mechanical dynamics. Our platform exhibits the intermodulation of two optical frequency combs in the gigahertz domain, resulting from self-sustained mechanical oscillations of a gigahertz PnC guided mode that interacts with a lasing megahertz breathing mode via the optical field, which occurs independent of thermal effects, as supported by our theoretical model.

The modulation frequency (Ω_1) can also be actively tuned even further via an external stimulus, such as an atomic force microscope tip or other static actuator which acts as a local perturbation with the dampening leading to an order of magnitude energy loss [43], or with additional electrostatic actuation as envisioned with electro-optomechanical systems [44,45]. In our case, this dampening would significantly shift *M1* and the modulation frequency by consequence. Regarding the spectral line shape, Miri *et al.* [40] demonstrated that this distribution can be readily controlled via the optical losses of the cavity, which can also be engineered and experimentally tuned. Such a modulation scheme further enhances understanding and versatility of high-frequency input-output phononic devices [46,47]. Control of the mechanical frequencies could be useful to realize harmonic locking [48] and enhance the optical frequency comb spectral span.

More generally, such a process enriches the level of control in multimode optomechanical platforms and could be used for applications such as realizing subthreshold multimode lasing of two gigahertz modes without the need for an external intermodal modulation of the laser [30]. Within this context, the extent to which the modulation frequency as well as the spectral distribution of the frequency comb lines can be readily controlled has yet to be studied, though such prospects could lead toward the realization of optomechanical logic gates [17].

ACKNOWLEDGMENTS

We acknowledge the support from the project LEIT funded by the European Research Council, H2020 Grant Agreement

No. 885689. ICN2 is supported by the Severo Ochoa program from the Spanish Research Agency (AEI, Grant No. SEV-2017-0706) and by the CERCA Programme/Generalitat de Catalunya. R.C.N. acknowledges funding from the EU-H2020 research and innovation programme under the Marie Sklodowska Curie Individual Fellowship (Grant No. 897148). O.F. is supported by a BIST Ph.D. fellowship under the Marie Sklodowska Curie Grant Agreement (No. 754558). M.A. and S.S. gratefully acknowledge funding from the Villum Foundation Young Investigator Program (Grant No. 13170), the Danish National Research Foundation (Grant No. DNRF147—NanoPhoton), Innovation Fund Denmark (Grant No. 0175-00022—NEXUS), and Independent Research Fund Denmark (Grant No. 0135-00315—VAFL).

[1] R. V. Laer, B. Kuyken, D. V. Thourhout, and R. Baets, Interaction between light and highly confined hypersound in a silicon photonic nanowire, Nat. Photon. **9**, 199 (2015).

[2] E. A. Kittlaus, W. M. Jones, P. T. Rakich, N. T. Otterstrom, R. E. Muller, and M. Rais-Zadeh, Electrically driven acousto-optics and broadband non-reciprocity in silicon photonics, Nat. Photon. **15**, 43 (2021).

[3] P. Krantz, M. Kjaergaard, F. Yan, T. P. Orlando, S. Gustavsson, and W. D. Oliver, A quantum engineer's guide to superconducting qubits, Appl. Phys. Rev. **6**, 021318 (2019).

[4] K. Fang, M. H. Matheny, X. Luan, and O. Painter, Optical transduction and routing of microwave phonons in cavity-optomechanical circuits, Nat. Photon. **10**, 489 (2016).

[5] L. Mercier de Lépinay, C. F. Ockeloen-Korppi, D. Malz, and M. A. Sillanpää, Nonreciprocal Transport Based on Cavity Floquet Modes in Optomechanics, Phys. Rev. Lett. **125**, 023603 (2020).

[6] S. Volz, J. Ordonez-Miranda, A. Shchepetov, M. Prunnila, J. Ahopelto, T. Pezeril, G. Vaudel, V. Gusev, P. Ruello, E. M. Weig *et al.*, Nanophononics: State of the art and perspectives, Eur. Phys. J. B **89**, 15 (2016).

[7] G. Ma, M. Xiao, and C. Chan, Topological phases in acoustic and mechanical systems, Nat. Rev. Phys. **1**, 289 (2019).

[8] X. Zhang, M. Xiao, Y. Cheng, M.-H. Lu, and J. Christensen, Topological sound, Commun. Phys. **1**, 97 (2018).

[9] R. C. Ng, A. El Sachat, F. Cespedes, M. Poblet, G. Madiot, J. Jaramillo-Fernandez, O. Florez, P. Xiao, M. Sledzinska, C. M. Sotomayor-Torres *et al.*, Excitation and detection of acoustic phonons in nanoscale systems, Nanoscale **14**, 13428 (2022).

[10] M. Aspelmeyer, T. J. Kippenberg, and F. Marquardt, Cavity optomechanics, Rev. Mod. Phys. **86**, 1391 (2014).

[11] C. Sanavio, V. Peano, and A. Xuereb, Nonreciprocal topological phononics in optomechanical arrays, Phys. Rev. B **101**, 085108 (2020).

[12] S. Barzanjeh, A. Xuereb, S. Gröblacher, M. Paternostro, C. A. Regal, and E. M. Weig, Optomechanics for quantum technologies, Nat. Phys. **18**, 15 (2022).

[13] M. Zhang, G. S. Wiederhecker, S. Manipatruni, A. Barnard, P. McEuen, and M. Lipson, Synchronization of Micromechanical Oscillators Using Light, Phys. Rev. Lett. **109**, 233906 (2012).

[14] H. Xu, D. Mason, L. Jiang, and J. Harris, Topological energy transfer in an optomechanical system with exceptional points, Nature (London) **537**, 80 (2016).

[15] F. Ruesink, J. P. Mathew, M.-A. Miri, A. Alù, and E. Verhagen, Optical circulation in a multimode optomechanical resonator, Nat. Commun. **9**, 1798 (2018).

[16] H. Xu, L. Jiang, A. Clerk, and J. Harris, Nonreciprocal control and cooling of phonon modes in an optomechanical system, Nature (London) **568**, 65 (2019).

[17] K. Pelka, G. Madiot, R. Braive, and A. Xuereb, Floquet Control of Optomechanical Bistability in Multimode Systems, Phys. Rev. Lett. **129**, 123603 (2022).

[18] D. Navarro-Urrios, N. E. Capuj, J. Gomis-Bresco, F. Alzina, A. Pitanti, A. Griol, A. Martínez, and S. Torres, A self-stabilized coherent phonon source driven by optical forces, Sci. Rep. **5**, 15733 (2015).

[19] D. Navarro-Urrios, N. E. Capuj, M. F. Colombano, P. D. García, M. Sledzinska, F. Alzina, A. Griol, A. Martínez, and C. M. Sotomayor-Torres, Nonlinear dynamics and chaos in an optomechanical beam, Nat. Commun. **8**, 14965 (2017).

[20] G. Arregui, M. F. Colombano, J. Maire, A. Pitanti, N. E. Capuj, A. Griol, A. Martínez, C. M. Sotomayor-Torres, and D. Navarro-Urrios, Injection locking in an optomechanical coherent phonon source, Nanophotonics **10**, 1319 (2021).

[21] P. E. Allain, B. Guha, C. Baker, D. Parrain, A. Lemaître, G. Leo, and I. Favero, Electro-Optomechanical Modulation Instability in a Semiconductor Resonator, Phys. Rev. Lett. **126**, 243901 (2021).

[22] K. E. Grutter, M. I. Davanço, and K. Srinivasan, Slot-mode optomechanical crystals: A versatile platform for multimode ptomechanics, Optica **2**, 994 (2015).

[23] P. E. Allain, L. Schwab, C. Mismer, M. Gely, E. Mairiaux, M. Hermouet, B. Walter, G. Leo, S. Hentz, M. Faucher *et al.*, Optomechanical resonating probe for very high frequency sensing of atomic forces, Nanoscale **12**, 2939 (2020).

[24] M. Sansa, M. Defoort, A. Brenac, M. Hermouet, L. Banniard, A. Fafin, M. Gely, C. Masselon, I. Favero, G. Jourdan *et al.*, Optomechanical mass spectrometry, Nat. Commun. **11**, 3781 (2020).

[25] W. Yu, W. C. Jiang, Q. Lin, and T. Lu, Cavity optomechanical spring sensing of single molecules, Nat. Commun. **7**, 12311 (2016).

[26] F. Marquardt, J. P. Chen, A. A. Clerk, and S. M. Girvin, Quantum Theory of Cavity-Assisted Sideband Cooling of Mechanical Motion, Phys. Rev. Lett. **99**, 093902 (2007).

[27] See Supplemental Material at http://link.aps.org/supplemental/10.1103/PhysRevResearch.5.L032028 for more details about theory, design, and for experimental and numerical methods.

[28] T. J. Kippenberg, H. Rokhsari, T. Carmon, A. Scherer, and K. J. Vahala, Analysis of Radiation-Pressure Induced Mechanical Oscillation of an Optical Microcavity, Phys. Rev. Lett. **95**, 033901 (2005).

[29] U. Kemiktarak, M. Durand, M. Metcalfe, and J. Lawall, Mode Competition and Anomalous Cooling in a Multimode Phonon Laser, Phys. Rev. Lett. **113**, 030802 (2014).

[30] L. Mercadé, K. Pelka, R. Burgwal, A. Xuereb, A. Martínez, and E. Verhagen, Floquet Phonon Lasing in Multimode Optomechanical Systems, Phys. Rev. Lett. **127**, 073601 (2021).

[31] A. B. Shkarin, N. E. Flowers-Jacobs, S. W. Hoch, A. D. Kashkanova, C. Deutsch, J. Reichel, and J. G. E. Harris, Optically Mediated Hybridization between Two Mechanical Modes, Phys. Rev. Lett. **112**, 013602 (2014).

[32] M.-A. Miri and A. Alù, Exceptional points in optics and photonics, Science **363**, eaar7709 (2019).

[33] O. Florez, G. Arregui, M. Albrechtsen, R. C. Ng, J. Gomis-Bresco, S. Stobbe, C. M. Sotomayor-Torres, and P. D. García, Engineering nanoscale hypersonic phonon transport, Nat. Nanotechnol. **17**, 947 (2022).

[34] M. Albrechtsen, B. Vosoughi Lahijani, R. E. Christiansen, V. T. H. Nguyen, L. N. Casses, S. E. Hansen, N. Stenger, O. Sigmund, H. Jansen, J. Mørk *et al.*, Nanometer-scale photon confinement in topology-optimized dielectric cavities, Nat. Commun. **13**, 6281 (2022).

[35] G. Arregui, R. C. Ng, M. Albrechtsen, S. Stobbe, C. M. Sotomayor-Torres, and P. D. García, Cavity Optomechanics with Anderson-Localized Optical Modes, Phys. Rev. Lett. **130**, 043802 (2023).

[36] G. Madiot, R. C. Ng, G. Arregui, O. Florez, M. Albrechtsen, S. Stobbe, P. D. García, and C. M. Sotomayor-Torres, Optomechanical Generation of Coherent GHz Vibrations in a Phononic Waveguide, Phys. Rev. Lett. **130**, 106903 (2023).

[37] Y. Li, J. Zheng, J. Gao, J. Shu, M. S. Aras, and C. W. Wong, Design of dispersive optomechanical coupling and cooling in ultrahigh-Q/V slot-type photonic crystal cavities, Opt. Express **18**, 23844 (2010).

[38] X. Luan, Y. Huang, Y. Li, J. F. McMillan, J. Zheng, S.-W. Huang, P.-C. Hsieh, T. Gu, D. Wang, A. Hati *et al.*, An integrated low phase noise radiation-pressure-driven optomechanical oscillator chipset, Sci. Rep. **4**, 6842 (2014).

[39] A. H. Safavi-Naeini, T. P. M. Alegre, M. Winger, and O. Painter, Optomechanics in an ultrahigh-Q two-dimensional photonic crystal cavity, Appl. Phys. Lett. **97**, 181106 (2010).

[40] M.-A. Miri, G. D'Aguanno, and A. Alù, Optomechanical frequency combs, New J. Phys. **20**, 043013 (2018).

[41] L. Mercadé, L. L. Martín, A. Griol, D. Navarro-Urrios, and A. Martínez, Microwave oscillator and frequency comb in a silicon optomechanical cavity with a full phononic bandgap, Nanophotonics **9**, 3535 (2020).

[42] M. L. Gorodetksy, A. Schliesser, G. Anetsberger, S. Deleglise, and T. J. Kippenberg, Determination of the vacuum optomechanical coupling rate using frequency noise calibration, Opt. Express **18**, 23236 (2010).

[43] J. Rieger, A. Isacsson, M. J. Seitner, J. P. Kotthaus, and E. M. Weig, Energy losses of nanomechanical resonators induced by atomic force microscopy-controlled mechanical impedance mismatching, Nat. Commun. **5**, 3345 (2014).

[44] L. Midolo, A. Schliesser, and A. Fiore, Nano-opto-electro-mechanical systems, Nat. Nanotechnol. **13**, 11 (2018).

[45] A. Pitanti, J. M. Fink, A. H. Safavi-Naeini, J. T. Hill, C. U. Lei, A. Tredicucci, and O. Painter, Strong opto-electro-mechanical coupling in a silicon photonic crystal cavity, Opt. Express **23**, 3196 (2015).

[46] S.-Y. Yu, X.-C. Sun, X. Ni, Q. Wang, X.-J. Yan, C. He, X.-P. Liu, L. Feng, M.-H. Lu, and Y.-F. Chen, Surface phononic graphene, Nat. Mater. **15**, 1243 (2016).

[47] H. Pirie, S. Sadhuka, J. Wang, R. Andrei, and J. E. Hoffman, Topological Phononic Logic, Phys. Rev. Lett. **128**, 015501 (2022).

[48] J. Zheng, Y. Li, N. Goldberg, M. McDonald, X. Luan, A. Hati, M. Lu, S. Strauf, T. Zelevinsky, D. A. Howe *et al.*, Feedback and harmonic locking of slot-type optomechanical oscillators to external low-noise reference clocks, Appl. Phys. Lett. **102**, 141117 (2013).